A Prototype Global Drought Information System Based on Multiple Land Surface Models

BART NIJSSEN,* SHRADDHANAND SHUKLA,+ CHIYU LIN,* HUILIN GAO,# TIAN ZHOU,* ISHOTTAMA,* JUSTIN SHEFFIELD,@ ERIC F. WOOD,@ AND DENNIS P. LETTENMAIER*

* *Land Surface Hydrology Group, Department of Civil and Environmental Engineering, University of Washington, Seattle, Washington*
+ *Land Surface Hydrology Group, Department of Civil and Environmental Engineering, University of Washington, Seattle, Washington, and Climate Hazards Group, Department of Geography, University of California, Santa Barbara, Santa Barbara, California*
# *Land Surface Hydrology Group, Department of Civil and Environmental Engineering, University of Washington, Seattle, Washington, and Water Resources Engineering, Zachry Department of Civil Engineering, Texas A&M University, College Station, Texas*
@ *Land Surface Hydrology Research Group, Department of Civil and Environmental Engineering, Princeton University, Princeton, New Jersey*

(Manuscript received 20 March 2013, in final form 25 March 2014)

ABSTRACT

The implementation of a multimodel drought monitoring system is described, which provides near-real-time estimates of surface moisture storage for the global land areas between 50°S and 50°N with a time lag of about 1 day. Near-real-time forcings are derived from satellite-based precipitation estimates and modeled air temperatures. The system distinguishes itself from other operational systems in that it uses multiple land surface models (Variable Infiltration Capacity, Noah, and Sacramento) to simulate surface moisture storage, which are then combined to derive a multimodel estimate of drought. A comparison of the results with other historic and current drought estimates demonstrates that near-real-time nowcasting of global drought conditions based on satellite and model forcings is entirely feasible. However, challenges remain because hydrological droughts are inherently defined in the context of a long-term climatology. Changes in observing platforms can be misinterpreted as droughts (or as excessively wet periods). This problem cannot simply be addressed through the addition of more observations or through the development of new observing platforms. Instead, it will require careful (re)construction of long-term records that are updated in near–real time in a consistent manner so that changes in surface meteorological forcings reflect actual conditions rather than changes in methods or sources.

1. Introduction

Smith and Katz (2013) report that during the period 1980–2011, droughts and heat waves ranked only behind tropical cyclones in the cost of damages associated with weather and climate disasters in the United States that individually caused more than a billion dollars worth of damage. This estimate did not include the 2012 drought, which covered much of the central United States. While the absolute magnitude of the economic losses is greatest in the developed world, the relative impact is much larger in the developing world, where agriculture typically occupies a larger percentage of the labor force and food insecurity is a major concern (Brown and Funk 2008). Given the magnitude of projected changes in drought from climate models (Dai 2011), the potential increase in susceptibility to droughts is alarming. Even though Sheffield et al. (2012) found little evidence indicating a change in the occurrence of drought events globally over the past 60 years, the Intergovernmental Panel on Climate Change stated in its 2007 report that "[d]rought-affected areas will likely increase in extent" (Parry et al. 2007, p. 11).

Nonetheless, our ability to monitor and predict the development and occurrence of droughts at a global scale

Corresponding author address: Bart Nijssen, Wilson Ceramics Lab, Rm. 111, Department of Civil and Environmental Engineering, Box 352700, University of Washington, Seattle, WA 98195-2700.
E-mail: nijssen@uw.edu

DOI: 10.1175/JHM-D-13-090.1

in near–real time is limited (Pozzi et al. 2013). The problem is particularly critical given that many of the most damaging droughts occur in parts of the world that are most deficient in terms of in situ precipitation observations. In recent years, a number of near-real-time drought monitoring systems have been developed with regional or global extent. For example, the University of Washington has operated a surface water monitor for the United States since late 2005 (Shukla et al. 2011; Wood 2008; Wood and Lettenmaier 2006), which uses station observations of temperature and precipitation to produce near-real-time estimates of drought conditions in terms of soil moisture (SM), snow water equivalent (SWE), and runoff, simulated by a suite of land surface models. The U.S. Drought Monitor (Svoboda et al. 2002) has provided weekly drought updates since 1999 as part of a partnership between the National Drought Mitigation Center at the University of Nebraska–Lincoln, the U.S. Department of Agriculture, and the National Oceanic and Atmospheric Administration. Kogan and Sullivan (1993) made an early attempt to develop a global drought monitor using satellite information, primarily using satellite-based vegetation indices. From 2007 to 2013, Lloyd-Hughes and Saunders (2007) operated a global drought monitor, which was updated on a monthly basis and used station-based precipitation from the Global Precipitation Climatology Centre (GPCC; Schneider et al. 2014) and air temperature from the European Centre for Medium-Range Weather Forecasts (ECMWF). Their system used the standardized precipitation index (SPI) and the Palmer drought severity index (PDSI). Princeton University operates an African drought monitor (Sheffield et al. 2014) as well as a global drought monitor (http://hydrology.princeton.edu), both of which are updated regularly and use satellite-based precipitation combined with temperature from the National Centers for Environmental Prediction's (NCEP) Global Forecast System (GFS) analysis fields. Drought conditions are reported as percentiles relative to a long-term climatology. Vicente-Serrano et al. (2010) operate a global drought monitor (http://sac.csic.es/spei/nuevo/map/maps.html) in which a monthly standardized precipitation evapotranspiration index (SPEI) is calculated based on monthly precipitation and potential evapotranspiration from the Climatic Research Unit (CRU) time series (TS) version 3.20 data (Jones and Harris 2012). Sohn et al. (2013) describe the development of a forecasting system for seasonal prediction of droughts and floods (www.apcc21.org), which uses a merged station and satellite-based dataset [Climate Anomaly Monitoring System–Outgoing Longwave Radiation (OLR) Precipitation Index (CAMS-OPI); Janowiak and Xie 1999] to calculate the SPI and output from multiple climate forecast models for seasonal forecast generation. AghaKouchak and Nakhjiri (2012) proposed a global drought monitor that uses satellite-based precipitation to report drought conditions based on the SPI. They implemented an approach in which near-real-time precipitation data from the Tropical Rainfall Measuring Mission (TRMM; Huffman et al. 2007) and Precipitation Estimation from Remotely Sensed Information Using Artificial Neural Networks (PERSIANN; Sorooshian et al. 2000) are made consistent with historical precipitation from the Global Precipitation Climatology Project (GPCP; Adler et al. 2003; Huffman et al. 2009) through the use of a Bayesian correction algorithm. This has evolved into the Global Integrated Drought Monitoring and Prediction System (GIDMaPS; Hao et al. 2014). Heim and Brewer (2012) describe the development of the Global Drought Monitor Portal, which is part of the Global Framework for Climate Services of the World Meteorological Organization and can act as a clearinghouse for global drought information from multiple sources.

In this paper we describe the implementation of a multimodel drought monitoring system, which provides near-real-time estimates of surface moisture storage for the global land areas between 50°S and 50°N with a time lag of about 1 day. In its current form, the system only monitors the moisture state of the system to study drought evolution and does not address impacts. The system is an extension of similar systems developed by our group for Washington State (Shukla et al. 2011) and for the United States (Wood 2008; Wood and Lettenmaier 2006). However, global application of the protocols used in the U.S. systems poses new challenges, particularly with respect to the generation of meteorological forcings that drive the land surface models used in such a system. The system is distinguished from other operational systems in that it uses multiple land surface models to simulate surface moisture storage, which are then combined to derive a multimodel estimate of drought.

2. Global Drought Information System

The Global Drought Information System (GDIS) combines hydrological simulations from multiple land surface models to provide daily estimates of near-real-time surface moisture conditions [SM, SWE, and total moisture (STOT), which is the sum of SM and SWE] at a spatial resolution of 0.5° between 50°S and 50°N. Surface moisture conditions are reported as percentiles relative to the simulated long-term climatology of each variable for the same grid cell and same day of the year. By expressing SM, SWE, and STOT as percentiles relative

to climatology, their values are normalized to fall between 0 and 100. A separate climatology is calculated for each of the land surface models to account for structural differences in the representation of soil moisture. The use of percentiles facilitates comparison between land surface models, between locations, and between times (our interest here is not the absolute amount of SM, SWE, and STOT, but to what extent they deviate from normal conditions at a given location and time).

GDIS consists of a suite of land surface models, an archive of historic forcings and associated model simulations, a method for constructing near-real-time forcings, and various analysis and display tools to assess and disseminate surface moisture conditions from which droughts can be inferred. Each of these components is discussed in the following sections.

a. Models and multimodel estimate

The land surface models used in the prototype GDIS are a subset of the models that are part of a regional drought monitor, which covers both the United States and Mexico and has operated at the University of Washington since late 2005 (Shukla et al. 2011; Wood 2008; Wood and Lettenmaier 2006). The specific choice of models is not a defining feature of GDIS. Additional land surface models can be added with relative ease, as long as the models can be operated in stand-alone mode and global model parameter datasets are available. In the version presented here, GDIS uses the Variable Infiltration Capacity (VIC) model (version 4.1.1; Liang et al. 1994), the Noah model (version 2.8; Ek et al. 2003; Mitchell 2005), and a grid-based version of the Sacramento (SAC) model (Anderson 1973; Burnash 1995; Burnash et al. 1973) to simulate SM, SWE, and STOT. The models use different representations of the subsurface. As implemented in GDIS, VIC uses three subsurface layers. The thickness of the individual layers varies from grid cell to grid cell, with soil and vegetation parameters as specified in Nijssen et al. (2001a,b). The Noah implementation uses four fixed-depth soil layers with a total soil depth of 2 m. The SAC model uses two soil layers composed of free and tension water storage, which contribute to evaporation and runoff. The free water storage of the lower layer is further divided into supplemental (fast) base flow and primary (slow) groundwater flow (Koren et al. 2003). In the GDIS implementation, the total depth of the upper layer varies from 71 to 135 mm, whereas the depth of lower layer varies between 285 and 541 mm. Global soil and vegetation parameters for Noah and SAC follow Koren (2006), Koren et al. (2003), and Mitchell (2005). The VIC model runs were performed in water balance mode using a daily time step, while Noah and SAC used a model time step of 3 h. All model output was aggregated to daily values and analyzed at daily or coarser time intervals.

Model-specific surface moisture estimates were converted to percentiles by comparing the simulated value for a given date and given location with a model climatology for the same day of year and model grid cell (Andreadis and Lettenmaier 2006; Shukla et al. 2011; Wood and Lettenmaier 2006). To ensure robust statistics, the percentiles are based on simulated values of those variables during the climatological period in a 5-day window centered on the target day of year.

Individual model estimates of SM, SWE, and STOT were combined into a single, daily multimodel estimate for each of the variables by averaging the percentiles from the individual models for each of those variables separately. The resulting daily multimodel time series was then treated the same way as the estimates from the individual models. That is, multimodel percentiles for each of the variables were calculated by comparing the multimodel value for a given date and given location with the multimodel climatology for the same day of year and model grid cell [method 2 in Wang et al. (2009)].

b. Meteorological forcings

Aside from logistical matters associated with the development and operation of any real-time system, the main challenge in the development of GDIS is the construction of meteorological forcing datasets that are spatially and temporally consistent. By definition, droughts exist within a climatological context. Drier-than-normal rather than dry is the operative part of the definition. Because observing platforms change over time and only limited sources of near-real-time meteorological forcings exist, either observed or modeled, it is invariably necessary to construct a long-term record from multiple data sources.

The real-time forcing data required for GDIS are daily precipitation, daily minimum and maximum temperature, and daily wind speed. Subdaily forcings, as well as downward shortwave radiation, downwelling longwave radiation, and relative humidity were generated using the mountain microclimate simulation model (MTCLIM) algorithm and disaggregation routines (Bohn et al. 2013; Kimball et al. 1997; Thornton and Running 1999) that form the meteorological preprocessor for the VIC model. These same forcings were then used as input to the Noah and SAC models. In addition to those forcings, the SAC model also requires potential evaporation as an input, which we generated using Noah. As a result, the operational sequence for our system is to run VIC first, followed by Noah, and finally SAC.

The single most important forcing is precipitation, which in our system is based on three separate datasets. The Sheffield et al. (2006, hereinafter S2006) forcing dataset, extended through 2008 and interpolated to a 0.5° spatial resolution, was used to perform the retrospective model runs that define the climatological period and the associated distribution of modeled soil moisture values. This dataset also includes daily wind speed and minimum and maximum air temperature.

The extended S2006 dataset ends at the end of 2008, after which we used the satellite-based TRMM Multisatellite Precipitation Analysis (TMPA) version 7 (V7) research quality product (RP) and real-time product (RT). The RP product incorporates station observations directly, while the RT product does not (although its calibration is based on station data). However, the RP product is only available with a time lag of a few weeks to months, while the RT product is available in near–real time.

Based on the source of the precipitation forcings, the model simulations can therefore be divided into three distinct periods: 1) a retrospective period based on the S2006 precipitation; 2) a spinup period, which uses the RP precipitation and which runs from the end of the retrospective period till a date in the recent past; and 3) a real-time period, which uses the RT precipitation and which runs from the end of the spinup period until about a day prior to current time. In a real-time system, the spinup period is periodically extended to take advantage of updates in the RP precipitation. The only part of the simulation that is run on a daily basis is the real-time period. Although it is strictly only necessary to run one additional day since the last update, we rerun the entire real-time period each day to take advantage of updates in near-real-time forcings (e.g., in case a particular field is posted late or is corrected and reposted).

For this paper, the retrospective period is from 1 January 1960 to 31 December 2008, which is also the period that is used to define the model climatology. That is, all reported percentiles are calculated with respect to the distribution of simulated values during this period. While it is possible to update the climatological period continuously, this makes it difficult to compare a percentile calculated on one date with one calculated on a later date. Rather than using a sliding window, we prefer to extend the reference period periodically at an interval of once a year or longer. For the purpose of this study, the climatological period is kept constant. The spinup period is from 1 January 2009 to 30 June 2012, while the real-time period is from 1 July to 31 December 2012.

In most cases, changes in data sources result in changes in model forcings because of the source-specific biases and errors in estimated precipitation. For example, the S2006 dataset, which makes extensive use of station observations, varies more smoothly (spatially) in areas with poor station coverage than the satellite data. Errors in satellite precipitation products and their potential impacts on hydrological simulations have been widely discussed in the literature (e.g., Hong et al. 2006; Hossain and Anagnostou 2006; Maggioni et al. 2011; Nijssen and Lettenmaier 2004).

To use the satellite-based precipitation products as forcings for GDIS, we have to amend their values in such a way that the modeled time series of surface moisture conditions are reflective of changes in actual precipitation rather than changes in the data source or observing platform. In effect, because our climatological period is based on the S2006 dataset, we have to make the RP and RT datasets consistent with S2006. If not, changes in precipitation that result from changes in platform may be misinterpreted as changes in drought conditions. This method has its drawbacks, in that any errors and biases in the S2006 dataset have to be imposed on the RP and RT products for the model to produce realistic percentiles. In addition, to achieve this consistency, a sufficiently long record of the spinup and real-time data sources must be available to create a mapping between those sources and the retrospective forcing dataset.

In our current GDIS implementation, the following method was used to achieve consistency between the TMPA V7 data sources and the S2006 data. The 3-hourly, 0.5° TMPA fields were aggregated to daily fields to match the temporal resolution of GDIS. We then applied monthly corrections to normalize the number of rainy days and mean precipitation amount. The number of rainy days is important, because the modeled hydrology is sensitive to the distribution of daily rainfall, and the MTCLIM algorithms use this information to estimate radiation and humidity. A systematic change in the number of rainy days will lead to systematic changes in these other forcings, which in turn will affect evapotranspiration and hence soil moisture dynamics.

The statistics used for normalization are based on the overlapping period between the TMPA and S2006 datasets. For the RP product this is the period from 1 January 1998 to 31 December 2008, while for the RT product it is from 1 March 2000 to 31 December 2008. The average number of rainy days was determined for each month of the year in each of the datasets for the overlapping period. If the average number of rainy days in the RP or RT dataset was greater than that in the S2006 dataset, a precipitation threshold was determined such that the number of rainfall events above the threshold in the RP or RT dataset equaled the number

of rainy days in the S2006 dataset. Any precipitation amounts below the threshold were simply discarded. No correction was made if the number of rainy days in the RT or RP product was less than in the S2006 dataset. To normalize the precipitation amounts, mean monthly ratios were calculated between the datasets. Spatial and temporal smoothing was applied to avoid abrupt changes in precipitation amounts and to make the ratios more robust. In particular, for each month and grid cell, a 3-month temporal window and a 2.5° spatial window (5 × 5 grid cells) were used to calculate the ratio. For example, to determine the June ratio for the grid cell centered at 40.25°N, 101.25°E, the average rainfall during the May–July period was calculated for the 25-cell area bounded in the southwest by 39°N, 100°E and in the northeast by 41.5°N, 102.5°E. The daily RP and RT fields were then corrected on a cell by cell basis by first setting the precipitation below the threshold to zero and then applying the ratio. This ensured that for the overlap period, the spinup and near-real-time datasets have the same (or fewer) number of mean monthly rainy days and the same mean monthly precipitation as the S2006 data.

After 2008, the air temperature forcings were taken from the Global Ensemble Forecast System (GEFS) reforecast project (Hamill et al. 2013), which provides global coverage and near-real-time daily updates. The reforecast project uses a ''frozen'' version of the GFS4 forecast model to create a daily forecast consisting of a control run and 10 ensemble members. Daily minimum and maximum temperature were based on the minimum and maximum 2-m air temperatures from the control run for the 0–24-h GEFS forecast interval and corrected so that the monthly mean values matched the monthly means from the S2006 dataset for the overlapping period (from 1 January 1985 to 31 December 2008). The correction applied the offset in the monthly mean for the overlap period to the daily time series of GEFS-based temperatures. Because the GEFS values are corrected to match the monthly means of the S2006 dataset, the selection of the control run rather than the ensemble mean is unlikely to affect the results.

Wind speed values post-2008 were set to the monthly mean values for the climatological period for each individual model grid cell. Thus, the wind speed values for a particular grid cell are the same for each day of the month and for the same month in subsequent years. Although this assumption affects evapotranspiration and daily variability, its effect on long-time soil moisture evolution is relatively small (Livneh et al. 2013).

c. *Nowcast generation*

All models were cold-started on 1 January 1948 (the start of the S2006 dataset) and run for the period from 1 January 1948 to 31 December 2008. The model state at the end of that run was then cycled twice through the period from 1 January 1948 to 31 December 1959 (again with the state at the end of the run recycled). Thus, in total, the model was spun up for 85 years before the start of the climatological simulation (from 1 January 1960 to 31 December 2008). The model state at the end of this period was used for the spinup simulation from 1 January 2009 to 30 June 2012. The model state at the end of that simulation was used to initialize the near-real-time simulation.

d. *System evaluation*

GDIS performance was evaluated by comparison with the U.S. Surface Water Monitor (SWM) operated by the University of Washington (UW) over the continental United States and Mexico and through its ability to simulate historic drought events during the climatological and spinup periods. The GDIS results were compared with the UW-SWM results, because high-quality gauge observations are available in the United States with which to force UW-SWM. In addition, we evaluated changes in model forcings and soil moisture dynamics during the spinup and real-time periods, which highlight challenges in the operation of a global, real-time system.

The 0.5° land mask is based on Jet Propulsion Laboratory (2013), with grid cells designated as land if more than half their area is land. In addition, following Sheffield et al. (2012), all desert regions with a mean annual precipitation of less than 0.5 mm day^{-1} (during the climatological period) were excluded from further analysis and have been masked in any spatial plots. In these areas, soil moisture values during the climatological period often have a very small dynamic range, and small absolute changes in precipitation can lead to large changes in percentile values. Since small changes in precipitation forcings persist between precipitation forcing datasets (even after correction), GDIS can show large persistent changes (both wetter and drier) for some of the desert regions (for example, in the Sahara). Most of these large differences are unlikely to be representative of actual changes in surface conditions.

3. Results and discussion

a. *Drought measure*

We used percentiles of STOT within a grid cell as our drought measure, with individual drought categories identical to those used in the U.S. Drought Monitor (Svoboda et al. 2002). Total moisture storage includes moisture within all soil layers in each of the individual models plus water stored on the surface in the form of

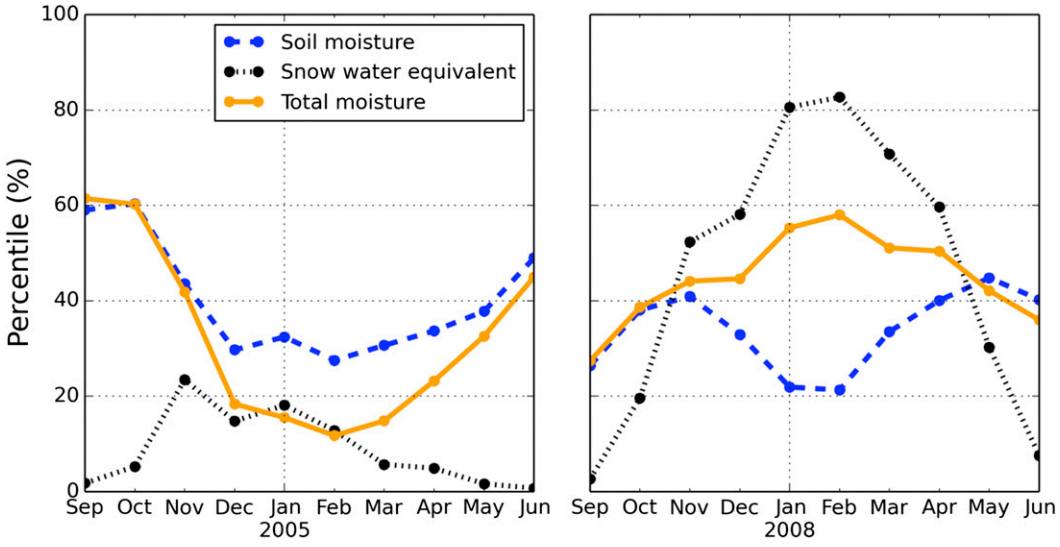

FIG. 1. Comparison of monthly SM, SWE, and STOT percentiles for western Washington State (area bounded by 45°–49.5°N, 119°–125°W) from the UW GDIS. (left) A case (2004/05) in which the SM percentiles are higher than the STOT percentiles because of a below-average snowpack; (right) the opposite case (2007/08). The STOT generally provides a more robust estimate of surface moisture conditions.

snow. While this distinction between soil moisture and total moisture makes no difference in areas where snow does not constitute a major component of the hydrological cycle, it provides a better indication of surface moisture status where snow is important. For example, Fig. 1 shows monthly time series of soil moisture, snow water equivalent, and total moisture percentiles over the western part of Washington State in the United States, an area where seasonal snow in the mountains provides an important source of moisture storage during the winter months. Reliance on the soil moisture percentiles leads to an underestimate of drought conditions when snow water equivalent is below normal (Fig. 1, left) and leads to an erroneous diagnosis of drought during periods when there is an anomalously large snowpack. We therefore show total moisture percentiles in all subsequent analyses. For areas without a seasonal snowpack, the soil moisture and total moisture values are identical. Note that in our operational drought monitors, we provide visualizations of all three variables separately (soil moisture, snow water equivalent, and total moisture percentiles).

b. Historic droughts

A reproduction of historic droughts is not an indication of the system's ability to provide meaningful nowcasts, but it is a necessary requirement, because it demonstrates that the combination of land surface models and meteorological forcing datasets results in an appropriate hydrologic response. The drought signal was examined both anecdotally (by verifying that the system captures severe droughts for specific regions) and numerically, the latter through a comparison with the UW-SWM. The UW-SWM uses some of the same models and also operates at a 0.5° spatial resolution, but it uses a different (station based) forcing dataset than is used by GDIS for the historic period. However, some of the underlying station information has been used in the construction of both the GDIS and UW-SWM forcing datasets.

An anecdotal comparison shows that GDIS captures major historic droughts and major wet episodes. For example, Fig. 2 shows the multimodel drought estimate for the same major droughts that are shown in Fig. 11 in Sheffield and Wood (2007). Low percentile values (reddish brown colors) indicate drought conditions, while high percentile values (dark green colors) indicate anomalously wet conditions. Note that by construct, the average multimodel percentile during the climatological period is 50% for any grid cell and any given day of the year. Figure 2 shows a spatial map of a major regional drought and a daily time series of the multimodel percentiles for the same region. The time series indicate not only periods of major drought, but they also identify major wet periods. For example, the time series for Australia (Fig. 2, bottom left) shows the anomalously wet periods in 1974/75, 2000, and 2011. The time series for Africa show less severe dry and wet periods, but this is simply a result of the larger averaging domain. Note that the figure is not identical to Fig. 11 in Sheffield and Wood (2007), where only the VIC model is used. For example, their panel for India shows a drought over all

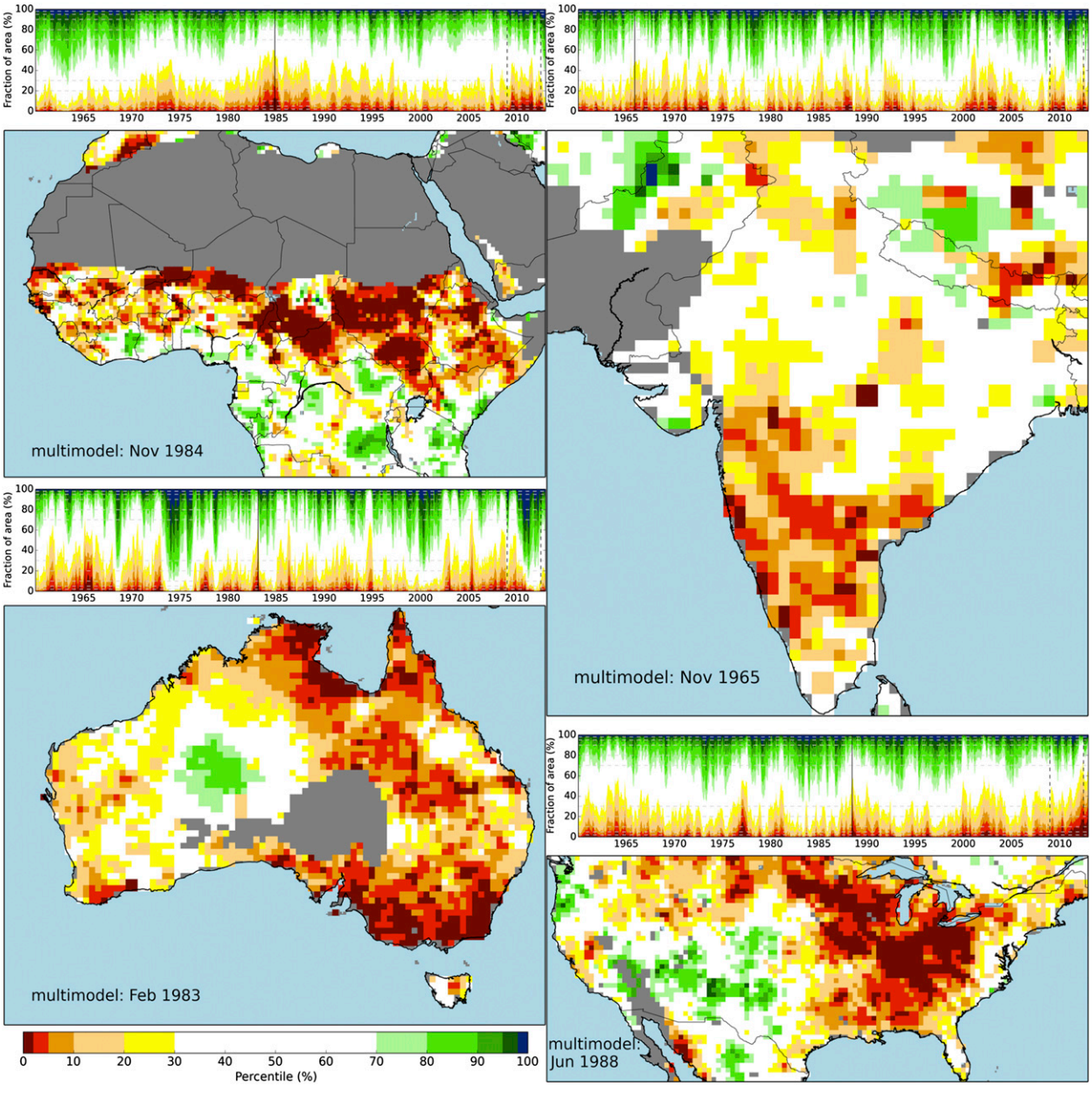

FIG. 2. Selected regional droughts. (top) The fraction of the area within a percentile range from 1 Jan 1960 to 31 Dec 2012. For example, the yellow band shows the fraction of the global land area for which the STOT on a given day falls within the 20th–30th percentile. The dashed horizontal lines indicate the percentiles that are used on the color bar. The spatial plots represent monthly mean percentiles for months in which significant droughts were reported. The vertical solid lines in the time series indicate the time of the spatial maps, while the vertical dashed lines correspond to 1 Jan 2009 and 1 Jul 2012. Compare with Fig. 11 in Sheffield and Wood (2007).

of Nepal in November 1965, while we only show a drought over the southern part of Nepal.

Figure 3 shows selected drought events (August 1988 and August 2012) for the United States, where we have results from the UW-SWM for comparison. Figure 3 (top) shows the daily time series of the multimodel percentiles over the continental United States simulated by UW-SWM (left) and GDIS (right). The figure is based on multimodel total moisture percentiles, with the UW-SWM estimate composed of more models than the GDIS estimate. Some of the differences result from the different climatological periods, forcings, and land surface models that are used by the two drought monitors, but they generally agree well on the occurrence of major droughts and wet episodes. However, there is a tendency for the GDIS results to show an increase in the

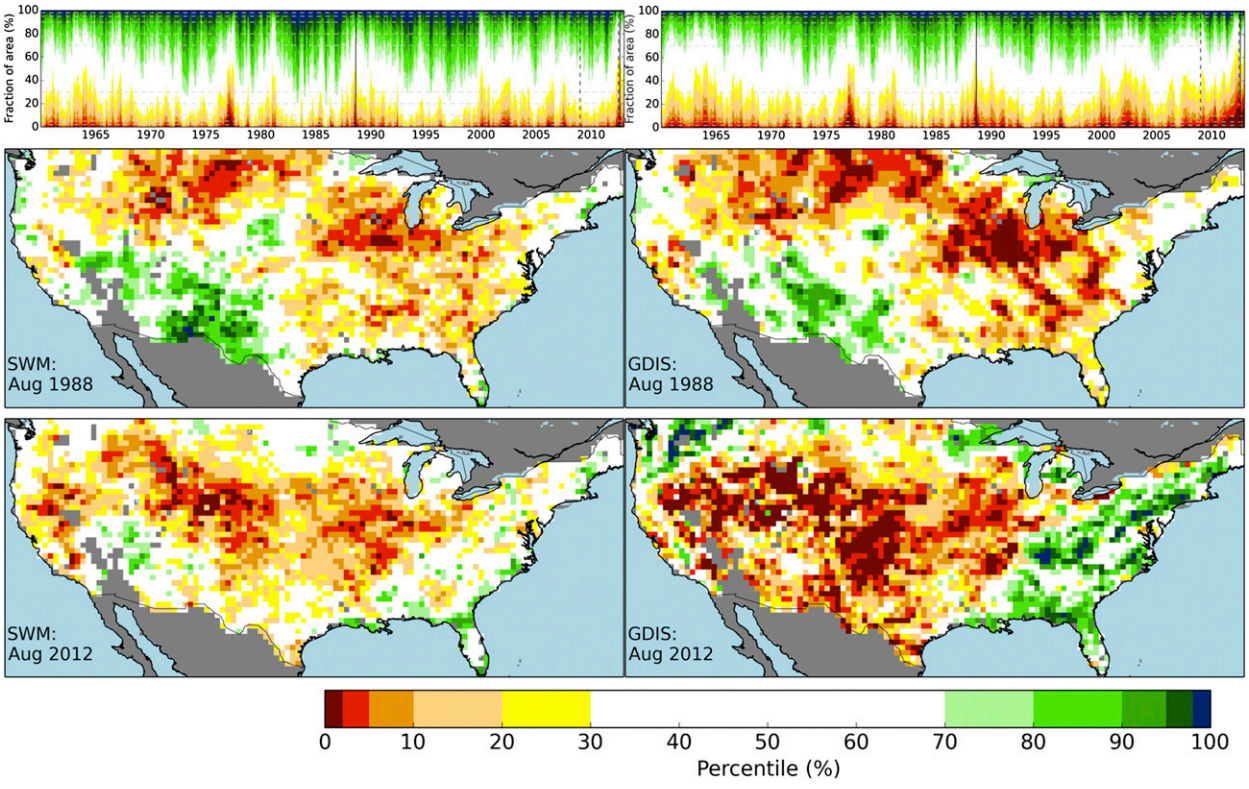

FIG. 3. Comparison of August 1988 and August 2012 drought conditions between the (left) UW-SWM and (right) GDIS. (top) The fraction of the United States within a percentile range from 1 Jan 1960 to 31 Dec 2012. The vertical solid lines in the time series figures indicate the time of the spatial maps, while the vertical dashed lines correspond to 1 Jan 2009 and 1 Jul 2012.

area that falls within the more extreme drought categories post-2008.

This increase in the area in extreme drought is not limited to the United States, but it is also apparent in the daily time series of the global land area (between 50°S and 50°N and masked as described above) that occupies a certain percentile range (Fig. 4). By design, during the climatological period, the percentile value for a given grid cell is less than or equal to 5% during 5% of the time. Consequently, on average during the climatological period, 5% of the land area has a total moisture percentile value less than or equal to 5%. However, we find that post-2008, there appears to be a persistent shift in the distribution, with about 10% of the area having a total moisture percentile value less than or equal to 5%. At the same time, we see a similar shift at the high end of the percentile range, with about 10% of the area with a percentile value equal to or greater than 95%. While major droughts and flooding occurred during this period, these shifts toward more extreme conditions on a global scale are mostly the result of a change in the source of the precipitation and temperature forcings. We discuss this in more detail in section 3e.

c. *Nowcast*

Figure 5 shows the instantaneous total moisture percentiles at the end of the 2008 (end of extended S2006 dataset) and at the end of 2012 for the entire GDIS domain. One clear change is in the smoothness of the plots. The extended S2006 dataset, which is used as the model forcings through the end of 2008, varies much more smoothly in space than the high-resolution satellite precipitation and model temperatures that are used post-2008. As a result, the soil moisture fields and hence the total moisture percentiles show greater spatial variability, resulting in increased graininess or image noise in the GDIS fields. Figure 6 shows a measure of the monthly mean image noise for the total moisture percentile and the meteorological forcings as a function of time. We have defined the image noise in the following way. For each grid cell, the average of the grid cell and its eight neighbors is subtracted from the grid cell value (all calculations were based on monthly time series). The standard deviation of all the differences across the domain is then taken as the image noise. The total moisture percentiles show a large increase in spatial variability post-2008, when satellite-based precipitation

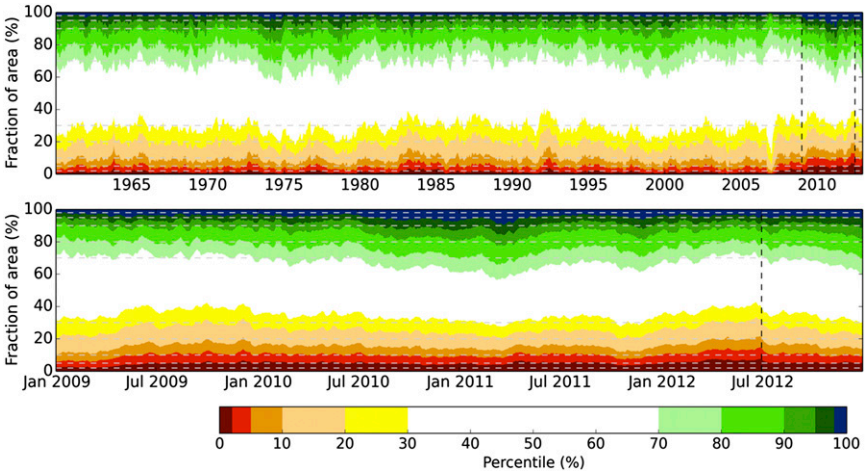

FIG. 4. Fraction of the global land area for which the total grid cell moisture is within a certain percentile range. (top) The entire period and (bottom) focusing from 1 Jan 2009 to 31 Dec 2012.

estimates (TMPA V7 RP) become the source of precipitation in GDIS. Another increase is seen after 1 July 2012, when TMPA V7 RT becomes the source of precipitation estimates. The differences between these two datasets are mostly the use of station data to correct the precipitation estimates in the RP product.

d. Multimodel drought estimates

One of the distinguishing features of GDIS is the use of multiple land surface models in tracking the evolution in total moisture storage at the land surface. While an in-depth evaluation of the performance of the individual models is not the topic of this paper, Fig. 7 shows the model spread on a seasonal basis for the period from March 1960 to February 2009. Model spread is defined as in Mo et al. (2012), except that we calculated the model spread on a seasonal rather than an annual basis and we used the deviation from the multimodel estimate rather than the deviation from the ensemble mean. That is, the variance of the seasonal intermodel spread Ω^s_{sp} for season s was calculated as

$$\Omega^s_{\mathrm{sp}} = \frac{1}{M \times T_s} \sum_{t=1}^{T_s} \sum_{m=1}^{M} S^2_m(t),$$

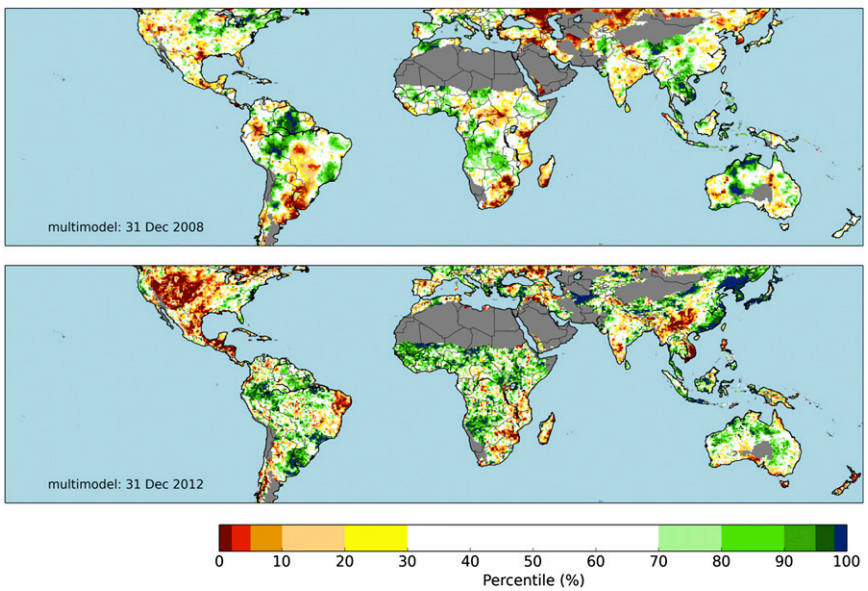

FIG. 5. GDIS total moisture percentiles for the entire domain at the end of (top) 2008 and (bottom) 2012.

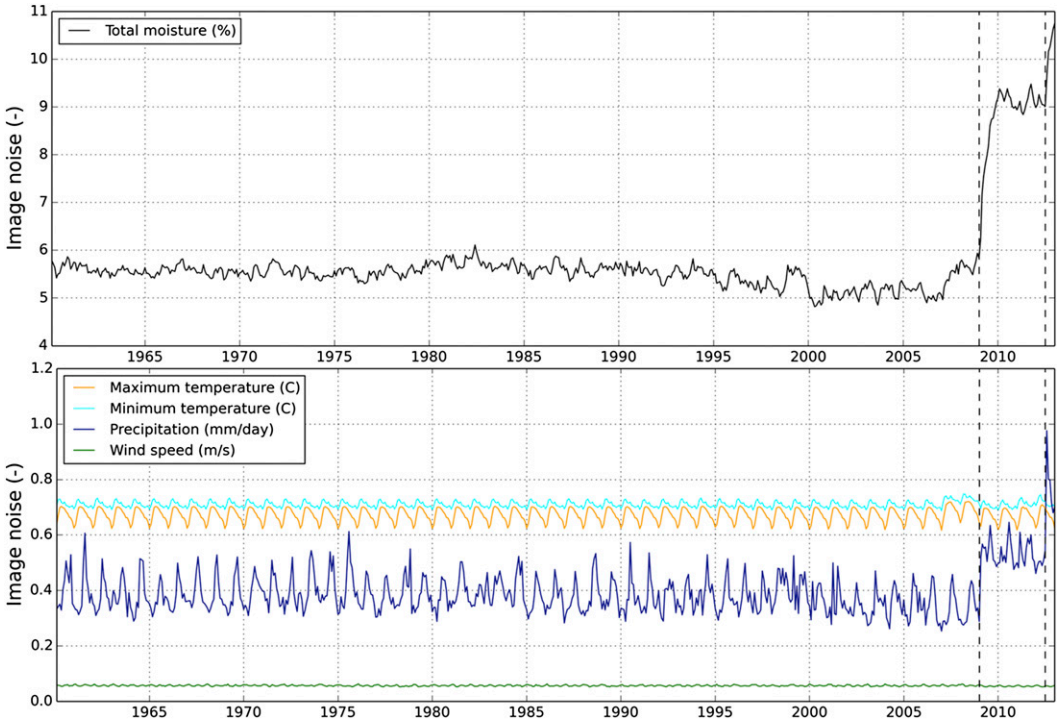

FIG. 6. Monthly mean image noise for (top) the total moisture percentiles and (bottom) the meteorological forcings. The vertical dashed lines correspond to 1 Jan 2009 and 1 Jul 2012.

where M is the total number of models in the ensemble, T_s is the total number of years during the climatological period (i.e., 1960–2008), and $S_m(t)$ is the deviation from the multimodel percentile of the drought index for model m in a given year t. This value was then normalized for each season by the interannual variance of the multimodel percentile Ω^s_{int} to provide the seasonal model spread $R^s = \Omega^s_{\text{sp}}/\Omega^s_{\text{int}}$. Because all models use the same meteorological forcings, the model spread results entirely from differences in model parameters and model parameterizations.

In general, the model spread is largest during the season when moisture storage is lowest. For example, model spread is highest in the western United States during June–August (JJA) and September–November (SON), when the modeled moisture values are dictated by the soil and evaporation parameterizations of the individual models rather than the precipitation forcings. Similarly, model spread is lowest during the rainy season in most areas with a distinct wet and dry season. For example, model spread is lowest in West Africa in JJA, in India during the monsoon season (JJA), and in northern Australia and the Mediterranean during December–February (DJF). In the humid tropics, the model spread tends to be low, although the model spread in central Africa is consistently higher than at the same latitude in South America or Oceania.

e. *Real-time precipitation and temperature forcings*

As described earlier, one of the main challenges in developing a near-real-time drought monitor is that droughts are defined with respect to a climatology. Consequently, realistic drought estimates require that the atmospheric forcings used in near–real time are consistent with the atmospheric forcings used to develop the climatology of modeled moisture storage values. As described in section 2b, we adjusted the near-real-time model forcings by matching monthly means for individual grid cells for the overlapping period of the various datasets (temperature and precipitation) and matching the number of rainy days for precipitation to the S2006 dataset. As a result, the global mean annual anomalies in the forcings during the post-2008 period are comparable to those during the pre-2008 period for all variables other than the minimum temperature (Fig. 8). The latter shows an increase during the post-2008 period that results in a reduction in the temperature range. Evaluation of the uncorrected temperature fields also shows an increase in the GEFS reforecast minimum temperatures over parts of the globe in the most recent years. While our correction procedure eliminates differences in the mean during overlapping time periods, it does not remove trends. The resulting reduction in the temperature range affects the

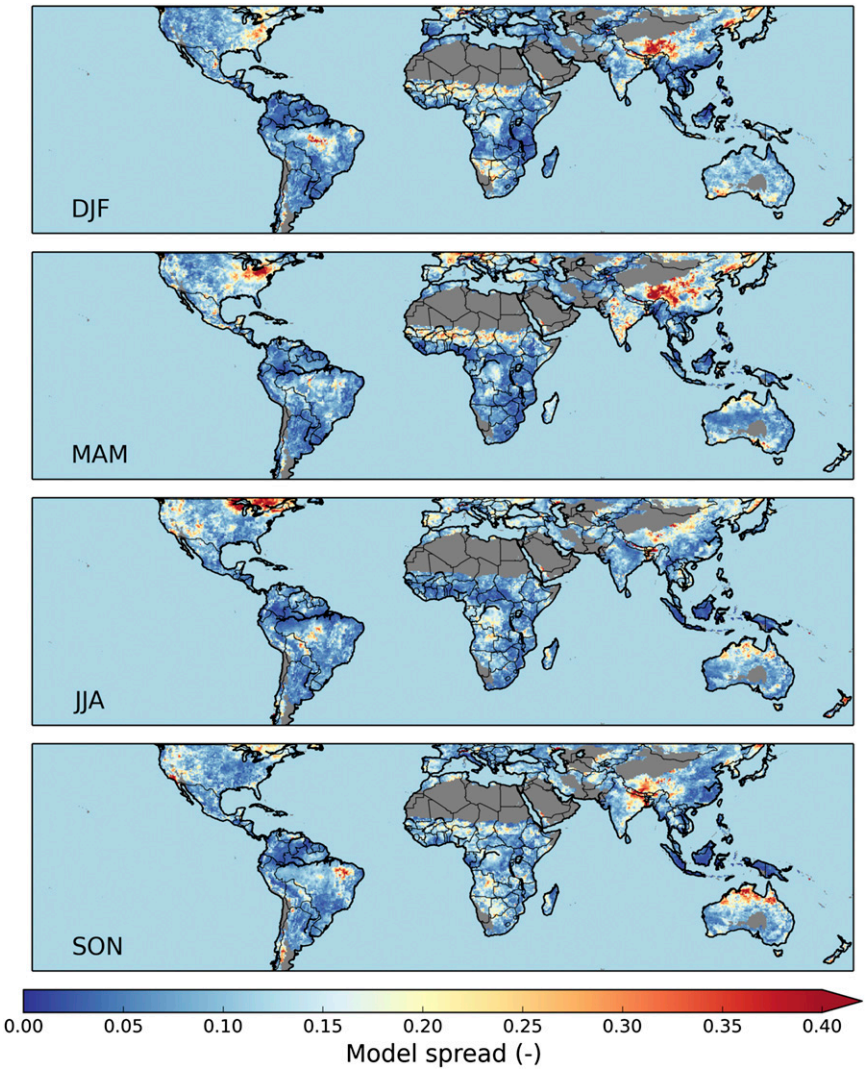

FIG. 7. Model spread on a seasonal basis for the period from March 1960 to February 2009.

hydrological simulations because incoming radiation, which is estimated using MTCLIM, is a function of the daily temperature range. A reduced range implies an increase in cloud cover and hence a reduction in incoming shortwave radiation and an increase in downwelling longwave radiation. The net effect is typically a reduction in the net radiation available for evapotranspiration and a small increase in moisture storage. This may explain in part the increase in areas with STOT percentiles greater than 90%.

However, most of the drought signal stems from the precipitation record, which in the global mean does not appear to be excessively wet or dry in the post-2008 period (Fig. 8). Yet, the global time series of STOT percentiles (Fig. 4) show an increase in the area covered by the highest (wettest) and lowest (driest) percentile categories, implying that a greater area of the globe is under extreme conditions post- than pre-2008. This increase in extremes highlights the challenges in creating a consistent forcing record rather than reflecting a true change in the occurrence of dry and wet grid cells. The increase in the spatial variability in the precipitation forcings post-2008 (Fig. 6) implies a change in the time series at individual grid cells, which may manifest itself in a shift toward percentiles more extreme than those for the climatological period. These extremes are then interpreted as an increase in the number of pixels in drought (or anomalously wet), but are essentially equivalent to a false positive. Because the percentiles are calculated with respect to a climatology for the same day and grid cell, small absolute changes in moisture storage during periods when the dynamic range of these values is small can result in large changes in the calculated percentiles.

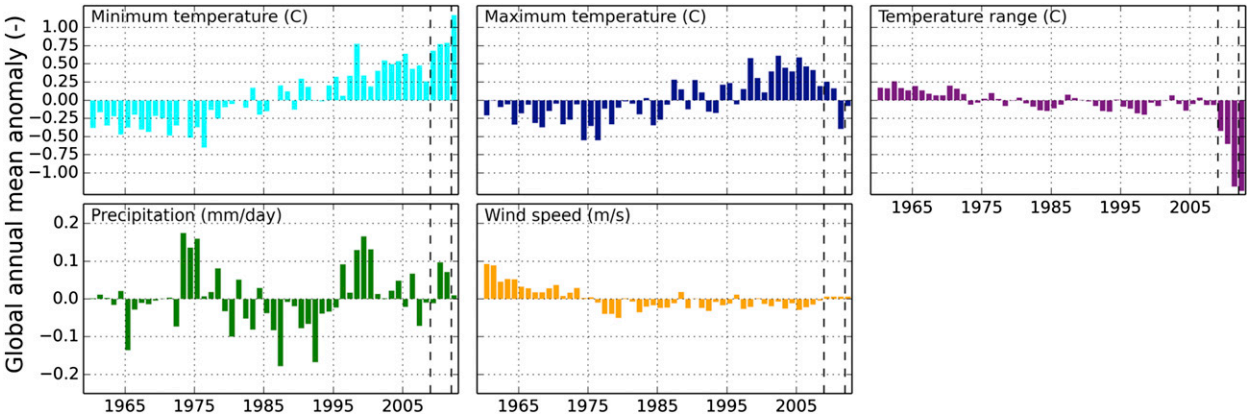

FIG. 8. Global mean annual anomalies (with respect to 1960–2008) for the meteorological forcings.

For example, Fig. 9 shows the monthly precipitation and temperature (top row) and the VIC simulated soil moisture and soil moisture percentile (bottom row) from 2000 through 2012 for a grid cell located in West Africa (Sahel). Note that for this location (14.75°N, 0.75°W) STOT is equal to SM since there is no snow. The years are color coded to allow a direct comparison of the annual cycle in each of the variables for individual years. The most obvious change in the post-2008 forcings is a reduction in the temperature range due to an increase in the minimum temperature (as discussed above). This reduction is strongest during the wet season. There is no strong shift in the annual precipitation and temperature cycle, with most of the precipitation occurring during July, August, and September and temperature maxima in April and November. However, there does appear to be a tendency for a slight increase in precipitation during September, October, and November. The combined results of the subtle changes in precipitation and temperature show an increase in modeled soil moisture for all months in the post-2008 period, particularly during the dry season when the dynamic range in modeled soil moisture is small. As a result, GDIS shows this area as anomalously wet during the dry season in the most recent years, something that is also apparent in Fig. 5, which shows anomalously wet conditions in the Sahel in December 2012.

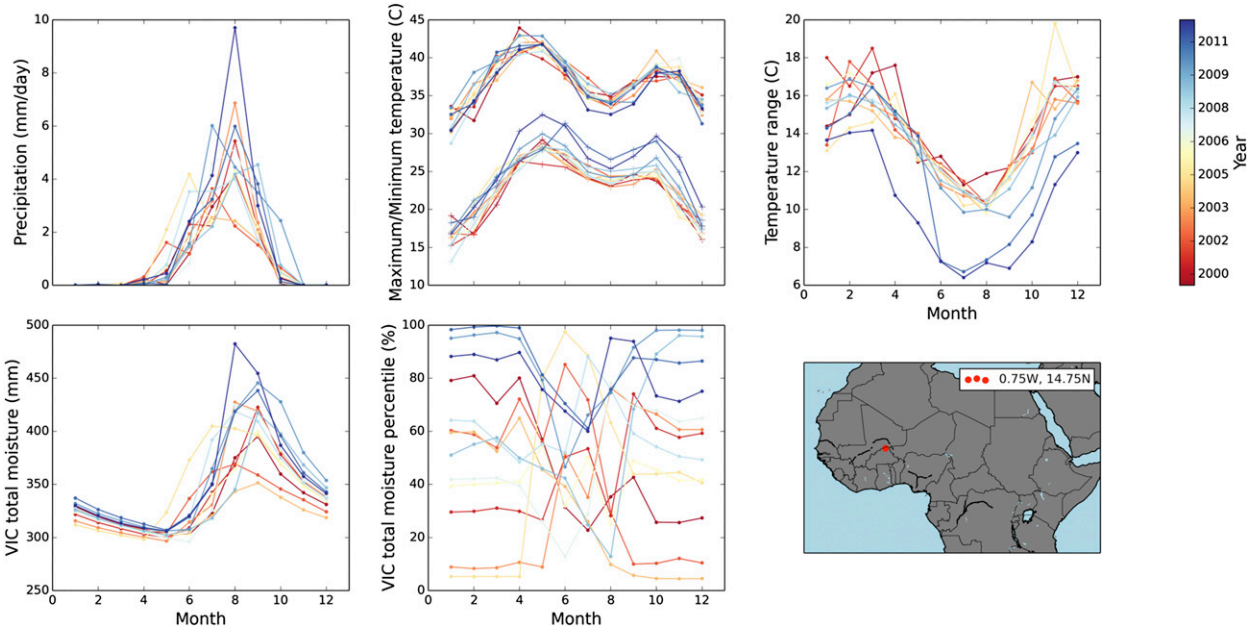

FIG. 9. (top) Mean monthly precipitation and temperature forcings and (bottom) VIC simulated SM and VIC STOT percentiles for a grid cell in West Africa for 2000–12.

The window size used to calculate the ratio between the S2006 and RP/RT precipitation (section 2b) also affects the precipitation record during the spinup and real-time period. For each month and grid cell, a 3-month temporal window and a 2.5° spatial window (5 × 5 grid cells) were used to calculate the ratio. The size of this window was largely motivated by the need to avoid precipitation totals equal to zero, so that robust correction ratios could be calculated given the short overlap between the different precipitation datasets, even in relatively dry areas. Because the corrections are applied on a monthly basis, the 3-month window was the shortest interval (longer than 1 month) centered on the current month. Figure 10 shows the effect of the choice of the window size on the ratio between S2006 and RP precipitation for January and July. Those grid cells for which the window-averaged RP precipitation was zero were assigned a ratio of 1 and are shown in white. The number of these grid cells (n) is shown on each panel. Larger spatial averaging windows (1 × 1, 3 × 3, and 5 × 5 cells) and longer temporal window sizes (1 and 3 months) result in smaller values for n but also result in significant smoothing of the ratios. During certain periods and in certain locations, the temporal smoothing process can change the ratios for a specific month and location from smaller than 1 to greater than 1 (for example, parts of South America in July during periods of low precipitation). The smoothing effects are particularly pronounced in areas with low precipitation (e.g., the Sahel region in January or southern Africa in July) and strongly affect the location shown in Fig. 9. Ratios are most strongly affected when precipitation is low. Consequently, the smoothing procedure has a limited effect on long-term precipitation totals, but it can affect moisture percentiles during periods where the moisture storage amounts exhibit a small dynamic range (Fig. 9).

While GDIS captures major droughts (like those in North America in 2012 and in the Horn of Africa in 2011–12), further improvement in the generation of near-real-time forcings will be required to reduce the misinterpretation of changes in the forcing datasets as droughts (or anomalously wet periods). Methods such as those proposed by AghaKouchak and Nakhjiri (2012), who use a Bayesian approach for matching historic and real-time datasets, and quantile mapping–based methods offer promise in this area. Alternatively, further refinement of the spatial and temporal window sizes used in calculating the ratios is possible and could be explored.

Uncertainties in GDIS drought estimates result from a number of sources. First and foremost is the uncertainty in precipitation forcings and the challenge in combining a near-real-time, satellite-based precipitation estimate with station-based precipitation fields for the climatological period. A large body of work exists that evaluates the impacts of uncertainty of satellite precipitation on hydrological simulations (e.g., Hossain and Anagnostou 2006; Nijssen and Lettenmaier 2004). Uncertainties in temperature forcings have a less severe impact on the drought estimates. However, systematic differences between the climatological and near-real-time period that cannot be corrected with a simple bias correction have the potential to result in systematic biases in drought estimates. The results are particularly sensitive to changes in the daily temperature range (maximum minus minimum temperature) because the MTCLIM algorithms use this quantity in the generation of the radiation forcings used by all the models. A change in the temperature range will be interpreted as a change in cloudiness and hence a change in radiation inputs, which in turn can affect evapotranspiration and soil moisture storage. Model errors form another source of uncertainty and are the motivation to develop a multimodel system. Clearly, as can be seen in Fig. 7, the model spread shows spatially coherent patterns of larger diversion, which require further evaluation. One challenge in evaluating the uncertainty of drought estimates is that no independent, direct measurement of drought exists that can serve as the reference value with which to compare model estimates. While it is generally possible to develop consensus whether a drought exists over a broad area, the uncertainty of drought category (or severity) for any particular location is generally much larger.

4. Conclusions

Near-real-time nowcasting of global drought conditions based on satellite and model forcings is entirely feasible, as demonstrated by GDIS and a number of other existing drought monitors with regional or global coverage that have been developed in the recent past. GDIS distinguishes itself from these other systems through the use of multiple land surface models, which are combined to produce a single, multimodel drought estimate. Despite difficulties in the creation of consistent meteorological forcings, GDIS is able to capture major drought events and track the progression of drought in near–real time.

However, challenges remain because hydrological droughts are inherently defined in the context of a long-term climatology. Changes in observing platforms invariably introduce changes in satellite precipitation products. These changes can in turn lead to surface moisture states that are anomalous compared to climatological conditions and hence can be misinterpreted

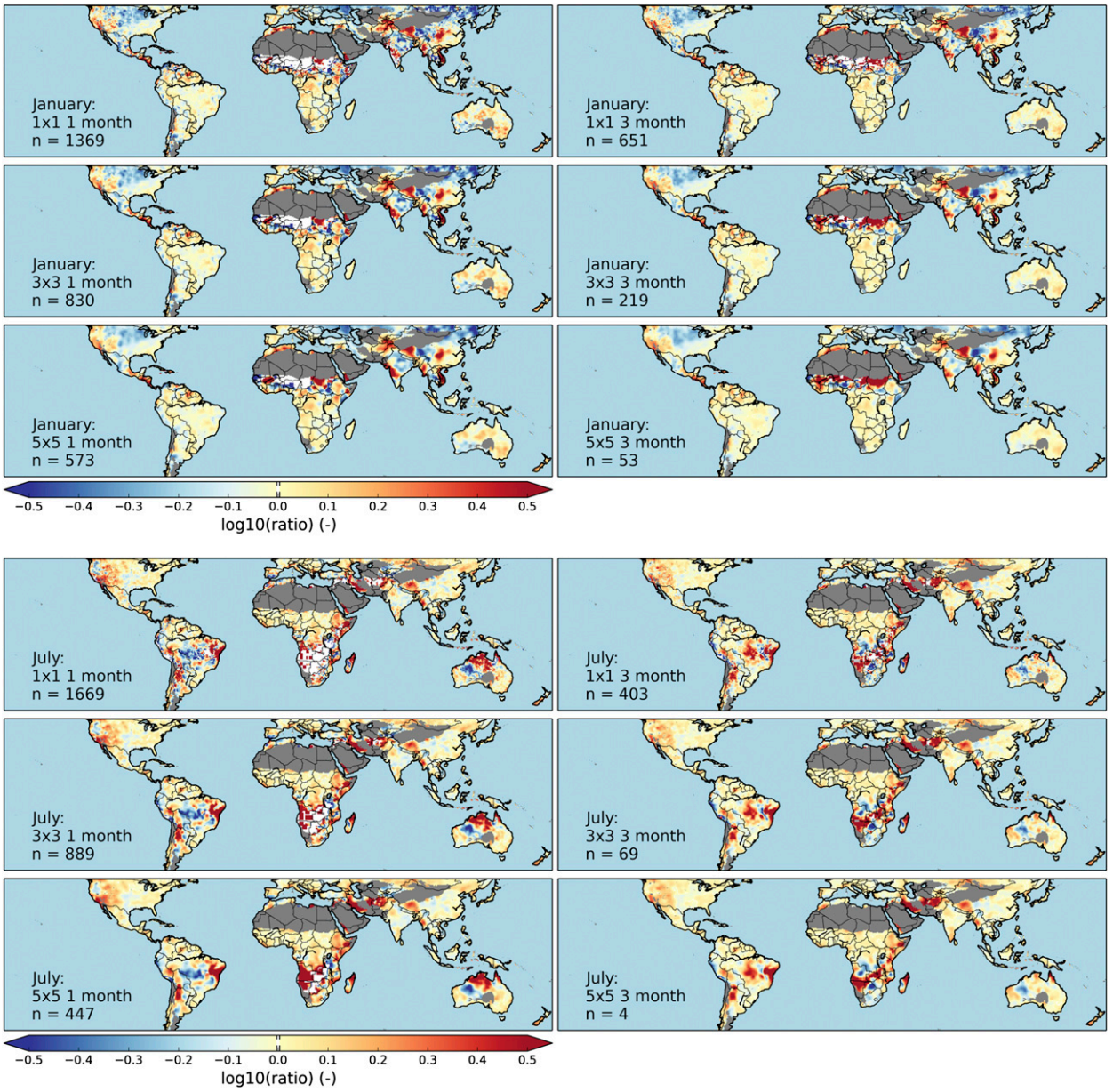

FIG. 10. Effect of window size on the ratio between the S2006 and RP datasets (S2006/RP) for (top) January and (bottom) July. The ratios are based on the period from January 1998 to December 2008 and are shown as a function of three spatial window sizes (1×1, 3×3, and 5×5 cells) and two temporal window sizes (1 and 3 months). Note that the ratio is set to 1 when the RP precipitation is zero. This is indicated by the grid cells that are white [log10(ratio) = 0]. The number of grid cells for which the ratio is set to 1 is indicated in each panel by *n*.

as droughts (or as excessively wet periods). Unfortunately, this problem cannot simply be addressed through the addition of more observations or through the development of new observing platforms. Instead, it will require careful (re)construction of long-term records that are updated in near–real time in a consistent manner so that changes in surface meteorological forcings reflect actual conditions rather than changes in methods or sources. Reanalysis and reforecast projects such as GEFS (Hamill et al. 2013) can be an important aid in this process, because they remove model updates as a source of change. However, because the underlying datasets that are assimilated are still subject to change, difficulties with the direct application of their products as a forcing for GDIS persist. There is a need for improved methods that combine long-term historical records,

which provide temporal continuity but have poor spatial coverage, with new observing and modeling platforms, which provide great spatial detail but lack a long-term climatology. Without such methods, it remains difficult to take advantage of new meteorological stations as well as new observation and modeling platforms in drought monitoring applications.

Finally, Fig. 7 clearly shows that even in a system where all models are forced with the same meteorology, significant differences in the simulated percentiles exist. While drought monitoring systems such as ours are able to capture droughts and their spatiotemporal evolution in broad terms, a formal evaluation of the drought categories simulated by different models and by different drought monitoring systems would be of interest. Mo et al. (2012) have provided a comparison for two of these systems for the United States, but this work needs to be expanded to a global context and combined with a formal evaluation of the simulated drought categories.

Acknowledgments. The University of Washington's contribution to this paper was supported under NASA Grant NNX10AG87G and NOAA Grant NA10OAR4310245 to the University of Washington. Shraddhanand Shukla is currently supported by the Postdoc Applying Climate Expertise (PACE) Fellowship Program, partially funded by the NOAA Climate Program Office and administered by the UCAR Visiting Scientist Programs.

REFERENCES

Adler, R. F., and Coauthors, 2003: The version-2 Global Precipitation Climatology Project (GPCP) Monthly Precipitation Analysis (1979–present). *J. Hydrometeor.,* **4,** 1147–1167, doi:10.1175/1525-7541(2003)004<1147:TVGPCP>2.0.CO;2.

AghaKouchak, A., and N. Nakhjiri, 2012: A near real-time satellite-based global drought climate data record. *Environ. Res. Lett.,* **7,** 044037, doi:10.1088/1748-9326/7/4/044037.

Anderson, E. A., 1973: National Weather Service River Forecast System—Snow accumulation and ablation model. NOAA Tech. Memo. NWS HYDRO-17, 87 pp. [Available online at ftp://ftp.wcc.nrcs.usda.gov/wntsc/H&H/snow/AndersonHYDRO17.pdf.]

Andreadis, K. M., and D. P. Lettenmaier, 2006: Trends in 20th century drought over the continental United States. *Geophys. Res. Lett.,* **33,** L10403, doi:10.1029/2006GL025711.

Bohn, T. J., B. Livneh, J. W. Oyler, S. W. Running, B. Nijssen, and D. P. Lettenmaier, 2013: Global evaluation of MTCLIM and related algorithms for forcing of ecological and hydrological models. *Agric. For. Meteor.,* **176,** 38–49, doi:10.1016/j.agrformet.2013.03.003.

Brown, M. E., and C. C. Funk, 2008: Food security under climate change. *Science,* **319,** 580–581, doi:10.1126/science.1154102.

Burnash, R. J. C., 1995: The NWS River Forecast System—Catchment modeling. *Computer Models of Watershed Hydrology,* V. P. Singh, Ed., Water Resources Publications, 311–366.

——, R. L. Ferrell, and R. A. McGuire, 1973: A generalized streamflow simulation system: Conceptual modeling for digital computers. Dept. of Commerce/NWS/CDWR Rep., 204 pp.

Dai, A., 2011: Drought under global warming: A review. *Wiley Interdiscip. Rev.: Climate Change,* **2,** 45–65, doi:10.1002/wcc.81.

Ek, M. B., K. E. Mitchell, Y. Lin, E. Rogers, P. Grunmann, V. Koren, G. Gayno, and J. D. Tarpley, 2003: Implementation of Noah land surface model advances in the National Centers for Environmental Prediction operational mesoscale Eta model. *J. Geophys. Res.,* **108,** 8851, doi:10.1029/2002JD003296.

Hamill, T. M., G. T. Bates, J. S. Whitaker, D. R. Murray, M. Fiorino, T. J. Galarneau, Y. Zhu, and W. Lapenta, 2013: NOAA's second-generation global medium-range ensemble reforecast dataset. *Bull. Amer. Meteor. Soc.,* **94,** 1553–1565, doi:10.1175/BAMS-D-12-00014.1.

Hao, Z., A. AghaKouchak, N. Nakhjiri, and A. Farahmand, 2014: Global integrated drought monitoring and prediction system. *Sci. Data,* **1,** doi:10.1038/sdata.2014.1.

Heim, R. R., and M. J. Brewer, 2012: The Global Drought Monitor Portal: The foundation for a Global Drought Information System. *Earth Interact.,* **16,** doi:10.1175/2012EI000446.1.

Hong, Y., K.-L. Hsu, H. Moradkhani, and S. Sorooshian, 2006: Uncertainty quantification of satellite precipitation estimation and Monte Carlo assessment of the error propagation into hydrologic response. *Water Resour. Res.,* **42,** W08421, doi:10.1029/2005WR004398.

Hossain, F., and E. N. Anagnostou, 2006: Assessment of a multidimensional satellite rainfall error model for ensemble generation of satellite rainfall data. *IEEE Geosci. Remote Sens. Lett.,* **3,** 419–423, doi:10.1109/LGRS.2006.873686.

Huffman, G. J., and Coauthors, 2007: The TRMM Multisatellite Precipitation Analysis (TMPA): Quasi-global, multiyear, combined-sensor precipitation estimates at fine scales. *J. Hydrometeor.,* **8,** 38–55, doi:10.1175/JHM560.1.

——, R. F. Adler, D. T. Bolvin, and G. Gu, 2009: Improving the global precipitation record: GPCP version 2.1. *Geophys. Res. Lett.,* **36,** L17808, doi:10.1029/2009GL040000.

Janowiak, J. E., and P. Xie, 1999: CAMS–OPI: A global satellite–rain gauge merged product for real-time precipitation monitoring applications. *J. Climate,* **12,** 3335–3342, doi:10.1175/1520-0442(1999)012<3335:COAGSR>2.0.CO;2.

Jet Propulsion Laboratory, 2013: ISLSCP II land and water masks with ancillary data. Oak Ridge National Laboratory Distributed Active Archive Center, Oak Ridge, TN, digital media, doi:10.3334/ORNLDAAC/1200.

Jones, P., and I. Harris, 2012: CRU TS3.20: Climatic Research Unit (CRU) time-series (TS) version 3.20 of high resolution gridded data of month-by-month variation in climate. Centre for Environmental Data Archival, Oxford, United Kingdom, digital media. [Available online at http://badc.nerc.ac.uk/view/badc.nerc.ac.uk__ATOM__ACTIVITY_3ec0d1c6-4616-11e2-89a3-00163e251233.]

Kimball, J. S., S. W. Running, and R. Nemani, 1997: An improved method for estimating surface humidity from daily minimum temperature. *Agric. For. Meteor.,* **85,** 87–98, doi:10.1016/S0168-1923(96)02366-0.

Kogan, F., and J. Sullivan, 1993: Development of global drought-watch system using NOAA/AVHRR data. *Adv. Space Res.,* **13,** 219–222, doi:10.1016/0273-1177(93)90548-P.

Koren, V., 2006: Parameterization of frozen ground effects: Sensitivity to soil properties. *Predictions in Ungauged Basins:*

Promises and Progress, M. Sivapalan et al., Eds., IAHS Publ. 303, 125–133.

——, M. Smith, and Q. Duan, 2003: Use of a prior parameter estimates in the derivation of spatially consistent parameter sets of rainfall–runoff models. *Calibration of Watershed Models,* Q. Duan et al., Eds., Water Science and Applications Series, Vol. 6, Amer. Geophys. Union, 239–254.

Liang, X., D. P. Lettenmaier, E. F. Wood, and S. J. Burges, 1994: A simple hydrologically based model of land-surface water and energy fluxes for general circulation models. *J. Geophys. Res.,* **99,** 14 415–14 428, doi:10.1029/94JD00483.

Livneh, B., E. A. Rosenberg, C. Lin, B. Nijssen, V. Mishra, K. Andreadis, E. P. Maurer, and D. P. Lettenmaier, 2013: A long-term hydrologically based dataset of land surface fluxes and states for the conterminous United States: Updates and extensions. *J. Climate,* **26,** 9384–9392, doi:10.1175/JCLI-D-12-00508.1.

Lloyd-Hughes, B., and M. A. Saunders, 2007: University College London Global Drought Monitor. [Available online at http://web.archive.org/web/20070210122816/http://drought.mssl.ucl.ac.uk/intro.html.]

Maggioni, V., R. H. Reichle, and E. N. Anagnostou, 2011: The effect of satellite rainfall error modeling on soil moisture prediction uncertainty. *J. Hydrometeor.,* **12,** 413–428, doi:10.1175/2011JHM1355.1.

Mitchell, K. E., 2005: The community Noah land surface model (LSM): User's guide, public release version 2.7.1. NCEP/EMC Doc., 26 pp. [Available online at http://www.emc.ncep.noaa.gov/mmb/gcp/noahlsm/Noah_LSM_USERGUIDE_2.7.1.htm.]

Mo, K. C., L.-C. Chen, S. Shukla, T. J. Bohn, and D. P. Lettenmaier, 2012: Uncertainties in North American Land Data Assimilation Systems over the contiguous United States. *J. Hydrometeor.,* **13,** 996–1009, doi:10.1175/JHM-D-11-0132.1.

Nijssen, B., and D. P. Lettenmaier, 2004: Effect of precipitation sampling error on simulated hydrological fluxes and states: Anticipating the Global Precipitation Measurement satellites. *J. Geophys. Res.,* **109,** D02103, doi:10.1029/2003JD003497.

——, G. M. O'Donnell, D. P. Lettenmaier, D. Lohmann, and E. F. Wood, 2001a: Predicting the discharge of global rivers. *J. Climate,* **14,** 3307–3323, doi:10.1175/1520-0442(2001)014<3307:PTDOGR>2.0.CO;2.

——, R. Schnur, and D. P. Lettenmaier, 2001b: Global retrospective estimation of soil moisture using the variable infiltration capacity land surface model, 1980–93. *J. Climate,* **14,** 1790–1808, doi:10.1175/1520-0442(2001)014<1790:GREOSM>2.0.CO;2.

Parry, M. L., O. F. Canziani, J. P. Palutikof, P. J. van der Linden, and C. E. Hanson, Eds., 2007: Summary for policymakers. *Climate Change 2007: Impacts, Adaptation and Vulnerability,* Cambridge University Press, 7–22.

Pozzi, W., and Coauthors, 2013: Towards global drought early warning capability: Expanding international cooperation for the development of a framework for global drought monitoring and forecasting. *Bull. Amer. Meteor. Soc.,* **94,** 776–785, doi:10.1175/BAMS-D-11-00176.1.

Schneider, U., A. Becker, P. Finger, A. Meyer-Christoffer, M. Ziese, and B. Rudolf, 2014: GPCC's new land surface precipitation climatology based on quality-controlled in situ data and its role in quantifying the global water cycle. *Theor. Appl. Climatol.,* **115,** 15–40, doi:10.1007/s00704-013-0860-x.

Sheffield, J., and E. F. Wood, 2007: Characteristics of global and regional drought, 1950–2000: Analysis of soil moisture data from off-line simulation of the terrestrial hydrologic cycle. *J. Geophys. Res.,* **112,** D17115, doi:10.1029/2006JD008288.

——, G. Goteti, and E. F. Wood, 2006: Development of a 50-year high-resolution global dataset of meteorological forcings for land surface modeling. *J. Climate,* **19,** 3088–3111, doi:10.1175/JCLI3790.1.

——, E. F. Wood, and M. L. Roderick, 2012: Little change in global drought over the past 60 years. *Nature,* **491,** 435–438, doi:10.1038/nature11575.

——, and Coauthors, 2014: A drought monitoring and forecasting system for sub-Sahara African water resources and food security. *Bull. Amer. Meteor. Soc.,* doi:10.1175/BAMS-D-12-00124.1, in press.

Shukla, S., A. C. Steinemann, and D. P. Lettenmaier, 2011: Drought monitoring for Washington State: Indicators and applications. *J. Hydrometeor.,* **12,** 66–83, doi:10.1175/2010JHM1307.1.

Smith, A. B., and R. W. Katz, 2013: US billion-dollar weather and climate disasters: Data sources, trends, accuracy and biases. *Nat. Hazards,* **67,** 387–410, doi:10.1007/s11069-013-0566-5.

Sohn, S.-J., C.-Y. Tam, and J.-B. Ahn, 2013: Development of a multimodel-based seasonal prediction system for extreme droughts and floods: A case study for South Korea. *Int. J. Climatol.,* **33,** 793–805, doi:10.1002/joc.3464.

Sorooshian, S., K.-L. Hsu, X. Gao, H. V. Gupta, B. Imam, and D. Braithwaite, 2000: Evaluation of PERSIANN system satellite–based estimates of tropical rainfall. *Bull. Amer. Meteor. Soc.,* **81,** 2035–2046, doi:10.1175/1520-0477(2000)081<2035:EOPSSE>2.3.CO;2.

Svoboda, M., and Coauthors, 2002: The Drought Monitor. *Bull. Amer. Meteor. Soc.,* **83,** 1181–1190.

Thornton, P. E., and S. W. Running, 1999: An improved algorithm for estimating incident daily solar radiation from measurements of temperature, humidity, and precipitation. *Agric. For. Meteor.,* **93,** 211–228, doi:10.1016/S0168-1923(98)00126-9.

Vicente-Serrano, S. M., S. Beguería, and J. I. López-Moreno, 2010: A multiscalar drought index sensitive to global warming: The standardized precipitation evapotranspiration index. *J. Climate,* **23,** 1696–1718, doi:10.1175/2009JCLI2909.1.

Wang, A., T. J. Bohn, S. P. Mahanama, R. D. Koster, and D. P. Lettenmaier, 2009: Multimodel ensemble reconstruction of drought over the continental United States. *J. Climate,* **22,** 2694–2712, doi:10.1175/2008JCLI2586.1.

Wood, A. W., 2008: The University of Washington Surface Water Monitor: An experimental platform for national hydrologic assessment and prediction. *22nd Conf. on Hydrology,* New Orleans, LA, Amer. Meteor. Soc., 5.2. [Available online at https://ams.confex.com/ams/pdfpapers/134844.pdf.]

——, and D. P. Lettenmaier, 2006: A test bed for new seasonal hydrologic forecasting approaches in the western United States. *Bull. Amer. Meteor. Soc.,* **87,** 1699–1712, doi:10.1175/BAMS-87-12-1699.